Sustainable Food Technology

ROYAL SOCIETY OF CHEMISTRY

PAPER

View Article Online
View Journal

Cite this: DOI: 10.1039/d6fb00019c

Optimisation of laminar jet flow microencapsulation variables to enhance the anthocyanin retention and antioxidant function of sohiong

Roshiya Nongmaithem,[a] Raju Sasikumar, *[a] Kaviarasu G.,[a] Selva Kumar T.,[ab] Ravikumar Rajarathinam,[b] Paras Sharma,[c] Sheena Haorongbam,[a] Kowsalya T.,[d] K. Senthilkumar[e] and Amit K. Jaiswal *[fg]

Anthocyanins are valuable dietary elements with biological functions and health-promoting effects. However, there are technological barriers to their use in the food industry, primarily due to their poor stability and susceptibility to environmental factors, such as oxygen, temperature, pH, and light, which can significantly affect the physicochemical characteristics of the final food products. In this study, the microencapsulation of an anthocyanin extract from sohiong fruits was performed using a laminar jet flow vibration nozzle, with calcium chloride as a hardening agent and sodium alginate as a polymer. To produce calcium-alginate microbeads with a high anthocyanin content and favourable morphological characteristics, an RSM approach was used. Thus, with three nozzles of 150, 300, and 450 μm, the effects of pressure, frequency, voltage, and distance to the gelling bath were adjusted. Alginate-loaded anthocyanin microbeads produced with a 300 μm (SA-A300) nozzle had an average size of 588 ± 43 μm, with a consistent spherical shape and a smooth surface. Similarly, the encapsulated sample (SF-A300) exhibited greater resistance to digestion and higher overall anthocyanin retention (84.33% ± 0.33%). In the simulated *in vitro* digestion (SIVD) environment, photo-oxidative and osmotic stress showed that (SA-A300) substantially preserved a high level of anthocyanins and demonstrated increased antioxidant activity. This optimisation improved the anthocyanin retention of sohiong, with great potential for use in the functional and nutraceutical industries, as well as other beverage sectors.

Received 17th January 2026
Accepted 12th March 2026

DOI: 10.1039/d6fb00019c

rsc.li/susfoodtech

Sustainability spotlight

This study highlights the sustainability potential of sohiong (*Prunus nepalensis*), an underutilised indigenous fruit, as a source of high-value anthocyanins for functional food and nutraceutical applications. The valorisation of sohiong supports agrobiodiversity, regional food systems, and improved utilisation of locally available plant resources that are often underexploited in mainstream food processing. The use of biodegradable, food-grade sodium alginate and a mild, laminar jet flow microencapsulation process enables the stabilisation and controlled release of anthocyanins while minimising thermal degradation and processing losses. By improving the gastrointestinal retention, antioxidant functionality, and resistance to osmotic and photo-oxidative stress, this approach enhances material efficiency and reduces the wastage of sensitive bioactive compounds. This work demonstrates a sustainable processing route for upgrading indigenous fruit-derived bioactives into stable functional ingredients, contributing to circular food innovation and supporting SDG 3 (Good Health and Well-Being) and SDG 12 (Responsible Consumption and Production).

1 Introduction

Prunus nepalensis belongs to the Rosaceae family and is a significant and underutilised native fruit species of North East India. It is a seasonal fruit commonly grown in the Khasi Hills, Jaintia Hills, and other parts of Meghalaya. The mature sohiong fruit, which is round and smooth, boasts a dark purple colour and possesses a unique flavour and taste. The round sohiong

[a]*Department of Agribusiness Management and Food Technology, North-Eastern Hill University, Tura Campus, Chasingre 794002, Tura, West Garo Hills, Meghalaya, India. E-mail: sashibiofoodster@gmail.com*

[b]*Center for Bioenergy and Bioproducts, Vel Tech Rangarajan Dr Sagunthala R&D Institute of Science and Technology, Avadi, Chennai 600 062, India*

[c]*Department of Food Technology, Mizoram University, Mizoram, India*

[d]*Department of Microbiology, School of Bioscience, Royal Global University, Guwahati, Assam-781035, India*

[e]*Department of Food Technology, Kongu Engineering College, Perundurai, Erode 638060, Tamil Nadu, India*

[f]*School of Food Science and Environmental Health, Faculty of Sciences and Health, Technological University Dublin, City Campus, Central Quad, Grangegorman, Dublin, D07 ADY7, Ireland. E-mail: amit.jaiswal@tudublin.ie*

[g]*Centre for Sustainable Packaging and Bioproducts (CSPB), Technological University Dublin, City Campus, Grangegorman, Dublin D07 H6K8, Ireland*

fruit transitions from green to pinkish colour and finally to a dark purple shade when it ripens, a change linked to its anthocyanin content, which is a natural pigment known for its potential health benefits.[1,2] Considering the abundance of bioactive substances and natural pigments found in this fruit, there is a possible prospect for its potential application in the food, pharmaceutical and various other sectors. This fruit remains underutilized despite its enormous economic potential, and its applications are limited to traditional and home-scale production.[3] The high levels of anthocyanins in the fruit, combined with other phytochemicals, exert synergistic effects that can influence physiological functions when applied widely in the food and nutraceutical industries.[4]

The stability of anthocyanins can be influenced by various factors, such as temperature, pH, concentration, and the presence of light, metal ions, enzymes, oxygen, or sulfur dioxide. Low stability, storage conditions, formulation, and colour loss are the primary barriers to the use of natural anthocyanins in the food sector.[5] Additionally, the processing conditions lead to unpleasant flavour, colour, and odour in the final product due to the issues with anthocyanin stability, thereby affecting their utilisation in different applications.[6] The health benefits of anthocyanins are highly affected by their bioavailability. This can be impacted by numerous factors, including their chemical structures, molecular sizes, the formation of glycosides or acylated forms, and interactions with other compounds.[7] The presence of food, gastric enzymes, bile acids, and gut microbes and the pH, motility and permeability of the gastrointestinal tract can affect the absorption of xenobiotics. Anthocyanin bioavailability and structure were studied in relation to the food complex and dietary constituents.[8] There is an increasing necessity for functional and nutraceutical foods derived from natural sources, as these can serve as alternatives to novel functional and nutraceutical options. A method for producing stable anthocyanins from natural sources is highly necessary.

Encapsulation technology has greatly improved the food industry by allowing the inclusion and stabilization of bioactive compounds in different food systems. This technique involves enclosing bioactive substances with a carrier material, which enhances their stability, bioavailability, and controlled release. Bioactive compounds, including vitamins, minerals, antioxidants, and probiotics, are valued for their beneficial health effects. Encapsulation not only preserves the functional characteristics of these compounds but also protects them from harmful environmental factors and interactions with other food ingredients.[9]

The laminar jet flow microencapsulation method is useful for encapsulating sensitive compounds, such as anthocyanins, due to its controlled fluid dynamics to produce highly uniform, monodisperse microcapsules, with high encapsulation efficiency and enhanced scalability, under gentle processing conditions.[10] Vibration technology, which involves disrupting a smooth liquid flow to create droplets through applied vibrations, has attracted considerable attention, primarily because it can generate uniform and monodisperse microspheres.[11] Comparing conventional approaches, this method affords uniform droplets and the ability to easily scale up, apply under sterile conditions, and regulate bead formation consistently. The spray drying encapsulation process uses high temperatures that denature anthocyanins and reduce their antioxidant activity and nutritional value.[11] Other traditional methods, such as standard extrusion and electrostatic extraction, are operated under low temperature, but their irregular bead sizes and difficulties in industry scaling up are the limitations. In contrast, laminar jet flow microencapsulation utilizes regulated vibration, frequency, and air pressure to transform a smooth liquid flow into uniform beads, thereby retaining bioactive compounds and facilitating large-scale application.[10]

Additionally, encapsulating anthocyanins using jet flow microencapsulation is widely applied in the food and nutraceutical sector. As a novel approach, this study aims to encapsulate anthocyanins from sohiong fruit through the jet flow microencapsulation. Using response surface methodology (RSM) and a central composite design (CCD), the optimal conditions for encapsulation, including nozzle size (μm), vibration frequency (Hz), electrode voltage (V), air pressure (mbar), and distance (mm), are determined. The response variables, such as encapsulation efficacy, yield, and microbead formations, are assessed. In addition, an *in vitro* gastrointestinal simulation activity was conducted to analyse the release behaviour of encapsulation and the retention of anthocyanin activity, along with their resistance to osmotic stress and photo-oxidation, which are typical challenges faced during storage and processing.

2 Materials and methods

2.1 Materials

Fresh, dark reddish *Prunus nepalensis* fruits were collected from Mairang (25°33′41.94″ N 91°38′9.67″ E), Meghalaya, India. Only ripe, soft-textured fruit was used in this study. The enzyme pectinase sourced from *Aspergillus aculeatus*, sodium alginate, calcium chloride ($CaCl_2$), sodium citrate, α-amylase, pepsin, pancreatin, porcine bile extract, sodium bicarbonate ($NaHCO_3$), potassium persulfate ($K_2S_2O_8$), ABTS [2,2-azino-bis(3-ethylbenzothiazoline-6-sulfonic acid)], DPPH (1,1-diphenyl-2-picrylhydrazyl), ferric chloride ($FeCl_3$), TPTZ (2,4,6-tripyridyl-*s*-triazine), sodium acetate, acetic acid, hydrochloric acid (HCl), sodium hydroxide (NaOH), sodium chloride (NaCl), potassium chloride (KCl), KH_2PO_4, and Na_2HPO_4 chemicals were purchased from Sigma-Aldrich in India.

2.2 Extraction preparation

The fruit seeds were removed using a hand knife; then, the pulp was collected and blended (Philips mixer, India) for subsequent analysis. The homogenous fruit pulp was treated with pectinase 0.1% w/v for 60 min at 150 rpm and 45 °C.[12] Based on the previous experiment by Sasikumar *et al.*[13] at various levels, the enzyme concentration and time were fixed. Microwave treatments were then performed at 600 W for 195 s. A high-end microwave extraction system (Milestone, Ethos X 49310, Italy) was used for the experiment. The microwave-treated pulp samples were manually compressed utilising a juice extractor.

The suspension obtained was passed through a double-layered muslin cloth for filtering. A lyophilizer (Alpha1-2 LD plus, Germany) was used to freeze-dry the filtrate that was extracted from the solution. To prevent photo-oxidation, it was sealed in an amber glass container and kept at ambient temperature for further experiments.

2.3 Estimation of total anthocyanin content (TAC)

The pH differential method described by Giusti and Wrolstad[14] was used to quantify the anthocyanin content in the freeze-dried sohiong fruit samples (SA-P). At pH 1.0, the anthocyanins are oxonium compounds, and they are colourless carbinols at pH 4.5. The samples (0.2 mg mL^{-1}) were gently combined with buffer solutions at pH 1.0 and pH 4.5, then allowed to incubate for 20 min at room temperature under dark conditions. The absorbance of each equilibrated sample was measured in 1-cm-pathlength cuvettes at 530 and 700 nm using a dual-beam UV-Vis spectrophotometer (Model: Genesys-S 10S UV-vis, Thermo Fisher, USA). Eqn (1) was used to determine the TAC content of the sohiong fruit, as follows:[15]

$$\mathrm{TA}\left(\frac{\mathrm{mg}}{\mathrm{mL}}\right) = \frac{A \times M_{\mathrm{w}} \times \mathrm{DF} \times L}{\varepsilon}, \quad (1)$$

where $A = (A_{510\ \mathrm{nm}} - A_{700\ \mathrm{nm}})\ \mathrm{pH}\ 1.0 - (A_{520\ \mathrm{nm}} - A_{700\ \mathrm{nm}})\ \mathrm{pH}\ 4.5$; V = volume of extract (mL), L = path length of the cuvettes (1 cm) and M = fresh mass of the sample (g).

2.4 Microbead formation process

A modified approach derived from Pasukamonset *et al.*[16] was employed to produce the microbeads. The microbeads were formed using a Buchi B-390 encapsulator [Flawil, Switzerland], which operates based on the vibrating nozzle technique. An example of the layout of the equipment is depicted in Fig. 1. Alginate was employed as the encapsulating agent at a concentration of 1.6% w/v for nozzles sized 150 μm (SF-A150), 1.7 %w/v for 300 μm nozzles (SF-A300), and 1.8% w/v for nozzles measuring 450 μm (SF-A300).[17] An equivalent volume of the SA-P (1 mg mL^{-1}) solution was mixed with sodium alginate and stirred at 45 °C in a magnetic stirrer (F91 T, FALC, Italy). A 100-mL suspension of alginate anthocyanins was injected into the feeding system using a syringe at a flow rate of 2.91 mL min^{-1}. Alginate-anthocyanin droplets transform from liquid droplets into solid beads when they fall into a hardening solution (0.2 M $CaCl_2$). In order to harden the beads, microcapsules were continuously stirred for 30 min using an agitator (F91 T, FALC, Italy).

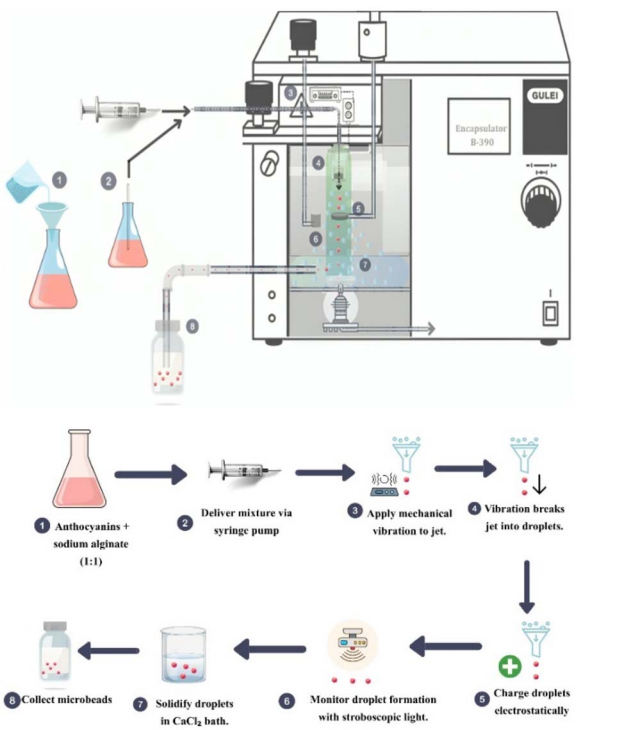

Fig. 1 Process flow of microbead formation using microencapsulation.

2.4.1 Optimization parameters and experimental design.

The encapsulator utilizes a stroboscopic lamp that is crucial for the real-time visualization of the bead formation, allowing the optimization of parameters essential for the bead formation. These parameters are optimized at a specific operating range that influences the size and shape of the beads. To ensure that the encapsulated bioactive are as protected as possible, the operation parameters of the equipment must be optimized.

Among all the instrumental factors that might influence the proper formation of microbeads, the vibration frequency (Hz) factor controls the rate at which the nozzle vibrates, which is important for the contravention of up of liquid jets into small beads. Voltage (V) is necessary to prevent the microbeads from coalescing by producing an extra electrostatic field between the nozzle and the hardening solution. The specified air pressure (mbar) for laminar flow was necessary to maintain a consistent laminar stream for the production of monodisperse beads. The variation in height from the nozzle tip to the $CaCl_2$ hardening bath affects the durability of the droplet shape. Nozzle size controls the droplet size and therefore directly influences the final bead size during formation.

Although RSM (response surface methodology) is an extensively used optimization tool, its application to laminar jet flow systems is non-trivial due to the sensitivity of the flow behaviour to the interacting parameters. A central composite design (CCD) with four factors and three levels was used to examine the response pattern and effectively optimize the combination of variables. This approach captures these interactions and provides a suitable optimization condition for consistent jet performance. The experimental design evaluated the influence of each variable across the corresponding ranges,[17,22] as outlined in Table 1. Totally, 30 experiments were conducted separately to obtain the experimental data. The three distinct dependent variables were analysed to determine the optimal conditions: (i) total yield (%) of the microbeads formed, (ii) well-formed spherical smooth microbeads (≥80% circularity), and (iii) percentage of encapsulation efficacy. The optimization process aimed to produce well-shaped microbeads, reduce the coalescence and tail formation of the beads and increase the encapsulation efficacy.

Table 1 Independent valuable ranges[17,22]

SI. No	Nozzle size (μm)	Vibration frequency (Hz)	Electrode voltage (V)	Air pressure (mbar)	Distance (mm)
1	150	100–2000	250–2000	140–320	30–150
2	300	100–1500	500–2000	56–200	30–150
3	450	100–1200	750–2000	40–80	30–150

2.4.2 Encapsulation efficiency. The efficiency of encapsulating TAC in the three different types of microbeads was assessed by combining them with a sodium citrate solution (2% w/w) in a 1 : 5 (w/w) ratio for 15 min. The encapsulated microbeads were mixed with sodium citrate solution, and the mixture underwent sonication for 30 min. Subsequently, the mixture was centrifuged at 1008×*g* for a duration of 10 min. The TAC in the citrate solution was measured by following the method described in section 2.3. The encapsulation efficiency was calculated using eqn (2):[18]

$$\mathrm{EE}(\%) = \frac{W_{\mathrm{O}}}{W_{\mathrm{I}}} \times 100, \quad (2)$$

where W_{O} = weight of loaded anthocyanins in microspheres and W_{I} = initial weight of anthocyanins.

2.4.3 Encapsulation yield. The encapsulation yield was determined by comparing the mass of the microbeads formed at the final stage of the procedure and the mass of the original encapsulated microbeads. These microbeads were rinsed, freeze-dried and powdered. The total yield (%) was calculated using eqn (3):[19]

$$\text{Encapsulation yield}(\%) = \frac{\mathrm{TAC}_{(\mathrm{EA})}}{\mathrm{TAC}_{(\mathrm{SE})}} \times 100, \quad (3)$$

where $\mathrm{TAC}_{(\mathrm{EA})}$ represents the total anthocyanin present in the encapsulated microbeads and $\mathrm{TAC}_{(\mathrm{SE})}$ represents the anthocyanin content in the alginate and extract mixture before encapsulation.

2.5 Morphological characterization of the encapsulated microbeads

2.5.1 Microbead size, shape and moisture. A digital micrometer and an optical microscope (BA-310, Motic, Germany) were utilized to assess the average size (n = 100) and shape of fresh wet microbeads (SF-A150, SF-A300, and SF-A450) using 4× and 10× magnification, respectively. The percentage of moisture content in the calcium alginate microbeads loaded with anthocyanins was evaluated through gravimetric methods in a vacuum oven at temperatures ranging from 35 °C to 40 °C until a stable weight was achieved.

2.6 Simulated *in vitro* digestion (SIVD)

In vitro replicas of digestive analysis were performed in accordance with the standardised procedure established by the COST Network consensus under FA1005 INFOGEST.[20] This methodology provides a consistent and physiologically relevant approach to replicate the human gastrointestinal system, allowing the assessment of the stability and bioavailability of the bioactive compounds under controlled circumstances. The limitations of this approach make it inappropriate for the comprehensive kinetic analysis of the various stages of digestion. Nevertheless, *in vivo* comparisons demonstrate a strong correlation with the INFOGEST method at the conclusion of each digestion phase. Therefore, the static model can be utilized to evaluate only digestion endpoints and not kinetics. These methods have recognized limitations and are unable to replicate the intricate dynamics of the digestion process or the physiological interactions with the host.[20]

To assess the outcome of SA-P and properly formulated microbead samples with anthocyanins, following expected ingestion, an analysis was performed across three different stages of digestion: the oral phase, which is represented by α-amylase to simulate oral conditions. The gastric phase was represented using pepsin and hydrochloric acid to imitate the environment of the stomach, and the intestinal phase utilized bile salts, pancreatin, and sodium bicarbonate to replicate the conditions found in the small intestine.[21] To make simulated saliva, 0.24 g of disodium phosphate, 0.02 g of monopotassium phosphate, and 0.80 g of sodium chloride were mixed with 100 mL of deionised water, and the pH was adjusted to 6.8. α-Amylase was added to the solution to reach an enzyme activity level of 200 U. Simulated gastric fluid was mixed with 0.32 g of pepsin derived from porcine gastric mucosa (pepsin A), along with 0.6 mL of hydrochloric acid (HCl) and 100 mL of 0.03 M sodium chloride (NaCl), and the pH was maintained at 1.2 by adding 1 M HCl. The simulated intestinal fluid prepared by the addition of 0.14 g of pancreatin and 0.86 g of porcine bile extract was combined, and the final solution was diluted to a total volume of 100 mL with 0.1 M $NaHCO_3$. The pH was subsequently adjusted to 7.4 by adding more 0.1 M $NaHCO_3$. Three stages of digestion were applied to the extracts. In the oral phase, 0.1 g of SA-P and a SF-A300 dried sample were mixed separately with 10 mL of saliva fluid (which contained α-amylase), and the mixtures were agitated in a water bath at 37 °C for 2 min at 120 rpm. During the gastric phase, the pH of the samples from the oral phase was adjusted to 2.0 by adding 5 M hydrochloric acid (HCl), followed by the addition of 10 mL of gastric fluid (which contained pepsin). The resulting mixtures were continuously agitated for 2 h in a shaking water bath at 37 °C. In the intestinal phase, 9 mL of intestinal fluid, consisting of pancreatin and bile salt, was combined with the digested samples from the stomach phase, and the pH was adjusted to 7.0 using 1 M sodium hydroxide (NaOH). Subsequently, 1.5 mL of sodium chloride solution and 1.5 mL of potassium solution were mixed, and the resulting solution was

kept in a shaking water bath at 37 °C for 2 h. After completing each stage of digestion, the enzymatic reactions were stopped by placing the samples in an ice bath (≈4 °C). At the end of each digestion process, the samples of the digested products were collected and centrifuged at 2500 rpm for 10 min. The resulting supernatants were separated and kept at −20 °C for further analysis. The simulated digestion experiments were conducted in triplicate. Control assays were performed under identical conditions, excluding digestive enzymes or bile salts. Following each digestion phase, the resulting digested samples were collected for the analysis of antioxidant capacity and the profile of anthocyanin compounds, facilitating comparison with the undigested samples.[22]

2.6.1 Estimation of antioxidant activity. The antioxidant activities (DPPH, ABTS and FRAP assays) of SA-P and a well-formed bead dried sample were assessed at each stage of SIVD analysis. Initially, 10 mg of both samples were dissolved separately in a sodium citrate solution (2% w/v) and sonicated for 20 min. After preparing the sample solutions at a 1 : 2 (w/v) ratio with distilled water, the solutions were centrifuged (2000×*g*, 15 min) and filtered.

In order to perform the DPPH (1,1-diphenyl-2-picrylhydrazyl) evaluation, 10 μL of the sample solutions was dissolved with 90 μL of ethanolic DPPH solution (0.2 mM in ethanol), and 3.9 mL of DPPH solution was added to 100 mL of ethanol as a positive control. A UV-Visible Spectrophotometer (Genesys 10S UV-Vis, Thermo Fisher Scientific, USA) was used to quantify the absorbance at 517 nm against a blank of ethanol. The percentage of DPPH radical inhibition was used to express the findings.[23]

The ABTS [2,2-azino-bis (3-ethylbenzothiazoline-6-sulfonic acid)] radical scavenging activity was evaluated following the method described by Mhlanga *et al.*[24] $ABTS^{\bullet}+$ solution, a combination of potassium persulfate stock solution (2.6 mM) and ABTS stock solution (7 mM), was incubated for 12–16 days at room temperature in a dark environment. After incubation, 2 mL of the stock solution was diluted with 54 mL of methanol to obtain an optical density (OD) of 0.7 ± 0.03 at 734 nm using a spectrophotometer, in comparison to a methanol blank. 90 μL of the $ABTS^{\bullet}+$ solution and 10 μL of the sample solution were mixed, and the optical density (OD) was measured at 734 nm. A standard curve was utilised to represent the trolox concentration (25–800 μM) and equivalent absorbance. The results were expressed as μmol TE g^{-1} sample.

The FRAP (Ferric Reducing Antioxidant Power) assay has been used to quantify the antioxidant potential of digested samples. A 300 mM acetate buffer (3.1 g of sodium acetate in 16 mL of acetic acid, pH 3.6), 10 mM ferric 2,4,6-tripyridyl-*s*-triazine (TPTZ) in 40 mM HCl, and 20 mM $FeCl_3$ made up the stock solution. The working solution was prepared by combining 25 mL of acetate buffer, 2.5 mL of TPTZ, and 2.5 mL of $FeCl_3$ in a 10 : 1 : 1 ratio. Volumes of 10 μL of the sample solution were combined with 90 μL of the FRAP solution, thoroughly mixed, and incubated for 45 min at 25 °C in the dark. After incubation, absorbance at 593 nm was measured with a spectrophotometer using 200 μL of the reaction mixture. Plotting a standard curve between the concentrations of ferrous sulphate heptahydrate ($FeSO_4 \cdot 7H_2O$) ranging from 0 to 1500 mg and their corresponding absorbance values yielded data represented as mg $FeSO_4$ g^{-1} sample.[25]

2.7 Osmotic and photo-oxidative stability of the encapsulated microbeads

In accordance with De Prisco *et al.*[26] the stability of the encapsulated microbeads in an osmotically challenged atmosphere was evaluated. The control sample consisted of non-encapsulated anthocyanins injected on the surface of empty microbeads. The anthocyanins released under stressful conditions were compared between the control and microbead samples after being subjected to an 80 °Brix TSS sugar solution for 180 min. After that, the solution was diluted and filtered in accordance with the instructions in section 2.3 for determining the total anthocyanin content. The microbeads were exposed to UV-C and photodegraded using the method outlined by Volf *et al.*[27] Encapsulated microbead samples were spiked with 100 mg of SF-A. This mixture was then combined with 10 mL of deionised water to create a homogeneous solution on a Petri plate. Separate encapsulated microbeads underwent a similar process. A photodegradation experiment was conducted on each sample solution for varying durations. Following each experiment, the solution was filtered, and its total anthocyanin content was determined using the method outlined in Section 2.3.

2.8 Statistical analysis

All experiments were conducted in triplicate. The results presented are expressed as means ± standard deviation (±SD, $n = 3$), as determined using Microsoft Office Excel, 2021. Statistical analysis was performed using SPSS (version 22.0, IBM Corporation, Armonk, NY, USA). Significant differences were assessed using ANOVA ($p < 0.05$). Normality was assessed using the Shapiro–Wilk test, while the homogeneity of variance was confirmed using Levene's test. The calculations and graphs as well as both single and multi-response optimizations were made using Design-Expert from Stat-Ease.

3 Results and discussion

3.1 Total anthocyanin content

The total anthocyanin was determined using the pH differential method, which is widely used in the food processing industry and is a simple method requiring only 20 min of incubation. The highest concentration of anthocyanin recorded was 2198.86 mg L^{-1}, achieved through a 0.01% enzyme concentration, enzyme incubation period of 60 min, 600 W of microwave power and 195 s of microwave exposure. Due to internal warming and cell disruption, the microwave extraction method improves the mass transfer rates of anthocyanin extraction from pulp. Kumar *et al.*[28] similarly studied several extraction methods for polyphenolic compounds from Black Soybean Seed Coat (BSSC). They found that the anthocyanin content in MAE was 5094.9 mg L^{-1}, suggesting that MAE is the most efficient extraction method when compared to enzyme-assisted extraction and conventional solvent extraction.

3.2 Optimization of microbead formation

Initially, multiple linear regression (MLR) was used to construct the response surfaces and account for the proportions of linear and squared terms as well as interactions between any two variables. CCD was used to optimise the formation of the alginate anthocyanin microbeads. To investigate the effects of vibration frequency (X_1), voltage (X_2), air pressure (X_3), and nozzle-to-bath distance (X_4) on the percentage of well-shaped microbeads with improved encapsulation efficiency, a second-order multiple linear regression (MLR) model was developed, including linear, quadratic, and two-variable terms. The low relative standard deviations for all responses confirmed excellent experimental reproducibility. Model adequacy was validated by ANOVA, which showed a non-significant lack-of-fit, indicating that model residuals were within the limits of pure experimental error, confirming high prediction accuracy (p < 0.05).

The proportion of well-formed microbeads and the high anthocyanin encapsulation efficacy showed a relative maximum at high voltage and frequency values as well as at low-pressure values, as shown in Fig. 2. The results of the dependent variable responses of yield percentage, percentage of well bead formation, and percentage of encapsulation efficacy of each sample, along with the optimised parameters, are shown in Table 2.

Among all samples, the 300 μm nozzle (SF-A300) exhibited the highest yield (89.18%), with well-formed beads at 84.68% and an encapsulation efficacy of 85.49%. It was achieved under optimum conditions, including a vibrational frequency of 1150.62 Hz, a voltage of 1250.2 V, and an air pressure of 120.15 mbar. While the nozzle-to-bath distance (X_4) did not substantially affect the bead morphology and was therefore fixed at 90 mm, the voltage (X_2), vibration frequency (X_1), and air pressure (X_3) had significant influences (p < 0.05). The meaningful two-variable interactions, especially frequency × voltage (X_1X_2) and frequency × pressure (X_1X_3), indicated that the final droplet shape was controlled by the coordinated adjustment of oscillatory instability and fluid dynamics. In fact, the multiple linear regression (MLR) analysis showed that voltage, frequency, and pressure were significant factors influencing the effective production of microcapsules (p-value < 0.05).

The distance from the nozzle to the hardening solution only affected the time it took for the bead to round before entering the $CaCl_2$ bath, which remained consistent across the experimental range, indicating that it was statistically non-significant. The jet flow vibration-microencapsulation method achieved an anthocyanin encapsulation efficiency of 85.49%, considerably overcoming the results from Mohammadalinejhad *et al.*[29] who used an alginate extrusion technique to encapsulate anthocyanins from purple corn. This enhancement was due to the simultaneous effects of vibrational breakup and electrostatic repulsion, which produced uniform microdroplets. The 150 μm nozzle also produced well-formed microbeads, with a yield of (86%) and EE (84%), but the microbead formation (78%) was relatively low due to the very high frequency and pressure, which caused irregular shapes. The 450 μm nozzle sample

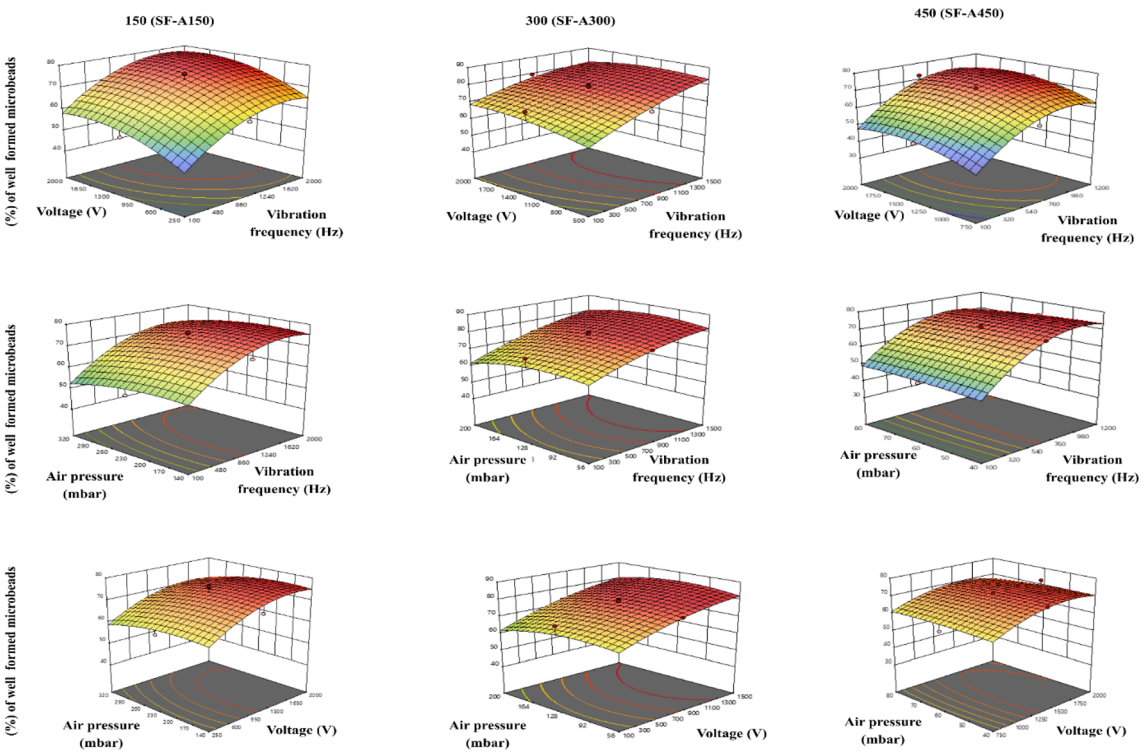

Fig. 2 Responses related to the key variables influencing the creation of spherical smooth microbeads evaluated based on the percentage of well-formed microbeads.

Table 2 Optimisation of the microbead production: operational variables and encapsulation outcomes across nozzle sizes

	Independent variables				Dependent variables		
Nozzle size (μm)	Vibration frequency (Hz)	Electrode voltage (V)	Air pressure (mbar)	Distance (mm)	Yield (%)	Microbead formation (%)	Encapsulation efficacy (%)
150 (SF-A150)	1552.31	1789.29	218.34	90	86.26	78.26	84.26
300 (SF-A300)	**1150.62**	**1250.20**	**120.15**	**90**	**89.18**	**84.68**	**85.49**
450 (SF-A450)	1045.31	1595.25	58.08	90	81.16	74.35	82.27

exhibited minimal performance, with low yield (81%) and bead uniformity (74%), though EE was 82%. Low-frequency (Hz) values were not effective enough to break the jet, leading to large droplets or to coalescence, which fell into the external hardening aqueous phase. Increasing the frequency leads to a more uniform jet break, resulting in consistent, well-defined drops. According to the Rayleigh–Plateau instability concept, uniform droplet breakup happened in the jet when the appropriate frequency aligned with the most unstable wavelength.[30] Mousavi and Siavashi[31] demonstrated that increasing the contact angle forms the optimal breakup frequency to achieve uniform beads. Integrating an electrostatic voltage system can reduce the coalescence effect by applying negative charges from string polymers onto the surfaces of the droplets, leading to a repulsion between them. Voltage improves the electrostatic repulsion between droplets, which adjusts the stability of internal and surface tension forces and efficiently increases the Weber number (W_e).[32]

The electrostatic potential can influence the microcapsule formation by attracting ions within the alginate solution to the surface of alginate droplets, which helps to counterbalance the surface tension at the interface between the droplet and needle tip, thereby decreasing the size of the droplets.[32] The formation of tails in the microbeads at increasing air pressures can be explained by rapid shear-induced breakup and by amplified Rayleigh–Taylor instability waves driven by high airflow pressure. These dimensionless groups provide a fluid-dynamics framework for interpreting the observed qualitative effects. In addition, this process leads to high droplet deformation and early breakdown. This phenomenon is most likely caused by the voltage-induced low droplet surface charge, which caused the beads to become homogenous and more likely to assemble. Instead, a voltage increase enabled the production of homogeneous, stable microcapsules with a high process yield.

3.2.1 Morphological characterisation of the encapsulated microbeads. The shape and structure influence the characteristics of alginate beads. Non-uniform diffusion within the microbeads leads to non-spherical beads. In addition, the shape of the microbeads affects the risk of an adverse foreign body reaction, which can lead to the eventual failure of the microbead system.[33] A total of 100 wet microbeads from each sample produced under these ideal circumstances were evaluated, and the average diameters were calculated. With the 150 μm, 300 μm, and 450 μm nozzles, the average sizes of the resulting wet microcapsules were 295 ± 12, 588 ± 43, and 896 ± 26 μm, respectively. When comparing the results, it was clear that the nozzle diameter has a significant influence on microbead size and moisture content.[34] As the nozzle size increased from 150 μm to 450 μm, the size of the resulting beads progressively increased.

The 300 μm nozzle produced microbeads with a 588 ± 43 size with a low moisture content of 2.606% ± 0.018%, demonstrating the best bead stability and bead uniformity. The moisture content of the microbeads showed only a slight decrease with the increase in the nozzle size, dropping from 2.868% for the smallest nozzle to 2.571% for the largest. The moisture contents of the anthocyanin samples from different microbeads are shown in Fig. 3. Almassri *et al.*[35] encapsulated β-glucosidase within alginate beads using a 750 μm nozzle, resulting in a consistent size for all the microbeads (<1000 μm). It was shown that increasing the nozzle size was directly proportional to the size of the beads.

3.2.2 Encapsulation efficacy. The overall anthocyanin content in the calcium alginate solution used for encapsulation, determined by accounting for alginate flow throughout the encapsulation process, was compared with the concentration of anthocyanins in the encapsulated capsules. Table 2 illustrates the efficiency of the anthocyanin encapsulation under varying conditions. Compared with SF-A150, SF-A300, and SF-A450, sample SF-A300 exhibited superior encapsulation effectiveness (85.49%). Corkovic *et al.*[36] encapsulated the total polyphenols from chokeberry in an alginate hydrogel using an encapsulator with a vibrating nozzle of 1000 μm, achieving an efficacy of approximately 39%. Our results suggested a comparatively better encapsulating efficacy in relation to the size of the nozzle. When compared to a 450 μm nozzle sample, smaller nozzles

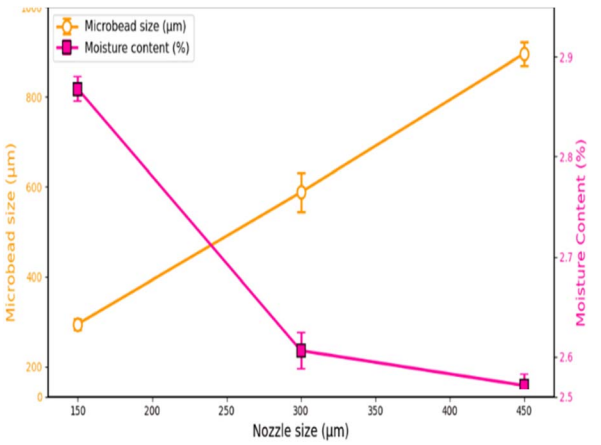

Fig. 3 Effect of nozzle size on the microbead size and moisture content.

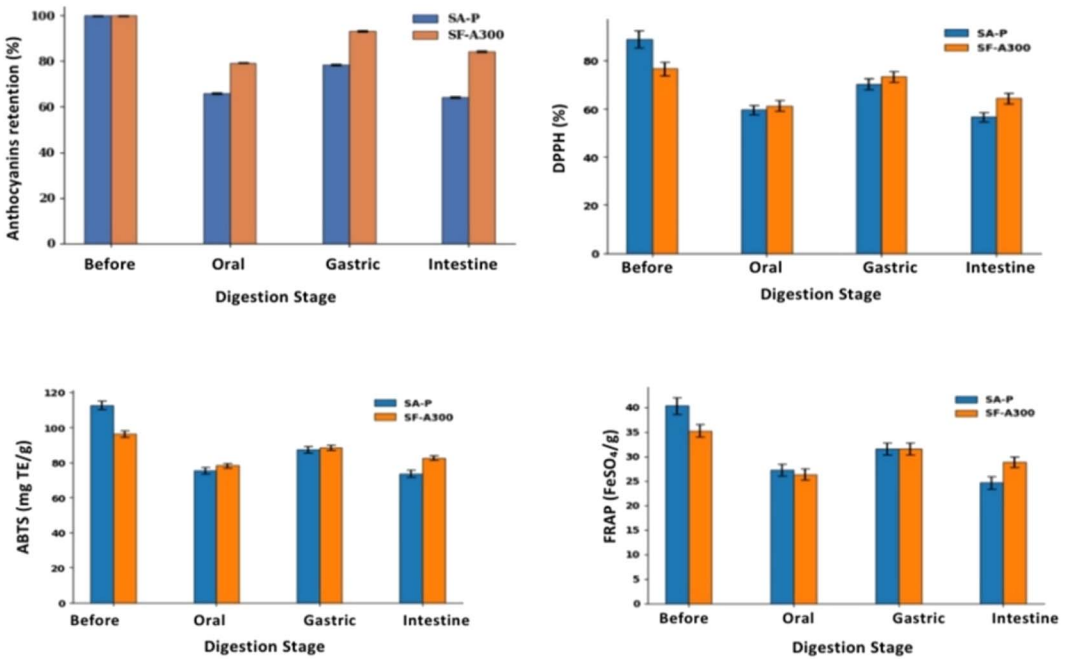

Fig. 4 Comparative antioxidant activity and anthocyanin retention of SA-P and SF-A300 during simulated digestion.

(150 μm) produced better encapsulation effectiveness due to droplet homogeneity under high vibration/air pressure. However, 300 μm nozzles demonstrated greater encapsulation efficacy under ideal conditions due to stable breakage that produced relatively small beads with optimum surface area-to-volume ratios.

Large nozzle diameters produced large microbead sizes, but the surface area-to-volume ratio dropped. As a result, more anthocyanins were released during the hardening phase of the microbeads, thereby improving the encapsulation efficiency.[37] The employed low-molecular-weight alginate was another factor contributing to the poor encapsulation efficiency. Compared with the low-molecular-weight microcapsules, those made with medium- or high-molecular-weight alginate had higher encapsulation efficiency. Nevertheless, the release rate of the active ingredient was substantially low, and the microcapsules were larger. Nevertheless, the release rate of the active ingredient is significantly slower, and the microcapsules are larger.[29]

3.3 Simulated *in vitro* digestion

Plants generally produce anthocyanins in glycosylated forms, which can enhance their stability and water solubility, thereby increasing their availability for intestinal transit.[38] Since the main functional component of the sohiong fruit is anthocyanin, the contents of the anthocyanin-extract microbeads could indicate how well they promote health.[39] The impact of physiological conditions on anthocyanins was examined by the *in vitro* simulations of intestinal digestion, and the recoveries of anthocyanins in intestinal and gastrointestinal digestion were computed. The anthocyanin content in non-encapsulated sohiong powder (SA-P) (2198.86 mg L^{-1}) was slightly higher than that of the dried encapsulated sohiong sample (SF-A300) (1843.6 mg L^{-1}), demonstrating the protective effect of the surrounding wall material.

Fig. 4 shows that after *in vitro* digestion (oral, stomach, and intestine), the SA-P sample retained 56.59% of its anthocyanin, while the SF-A300 sample retained 73.86%. These findings are better than those from the study reported by Fredes *et al.*,[40] who showed that the retention of anthocyanin in maqui juice microparticles made with inulin and alginate was 43% and 44%, following *in vitro* digestion. Compared with the non-encapsulated sohiong (SA-P), the encapsulated sohiong sample (SF-A300) exhibited much greater retention of individual anthocyanin during the simulated digestion. The physical barrier function of the microcapsule matrix, which lowered pigment exposure to pH fluctuations, digestive enzymes, oxygen, and bile salts and ensured a slower, more regulated release during digestion, was responsible for the improved performance.[41]

The result demonstrates the relative stability of the anthocyanin in the encapsulated sohiong under digestive conditions. At a pH of 2 or lower, anthocyanin predominantly existed as the coloured flavylium cation form; as a result, a substantial amount of natural pigments was preserved during the stomach stage. Following the increase in pH to 7–8, ring-opening changes induced by exposure to pancreatin and bile salts caused anthocyanins to shift toward an unstable colourless chalcone pseudo-base.[42]

The anthocyanin content of the non-encapsulated powder dropped dramatically from the oral stage of digestion. However, under gastric acidity, there was a partial stabilisation, increasing retention to 64.28% ± 0.29%, before a significant decline in the intestinal phase. The encapsulated sample (SF-A300), on the other hand, showed more resistance throughout

digestion, resulting in an overall retention of anthocyanins of 84.33% ± 0.33%. Fig. 4 demonstrates that the encapsulated sample exhibited the controlled release of anthocyanins in gastrointestinal tract delivery systems. The results of the study showed that encapsulation had a greater ability to inhibit anthocyanin degradation, which might increase the bioaccessibility of the chemicals in the digestive system.[43]

The antioxidant activities of undigested and digested (encapsulated or non-encapsulated) samples were evaluated using DPPH, FRAP, and ABTS, and the values are displayed in Fig. 4. The DPPH assay activity decreased by 36.32% after intestinal digestion, but the SF-A300 sample only lost 15.86% of DPPH activity. Calcium alginate matrix production reduced pigment exposure to pH fluctuations, digestive enzymes, oxygen, and bile salts, thereby ensuring a relatively slow and controlled release during digestion.[37] This indicated the stabilization of electron-donating structures in the retention of the encapsulated samples, as reflected in the ABTS (86.30%) and FRAP (82.06%) assay results. The results highlighted the relative stability of anthocyanins in encapsulated sohiong (SF-A300) under gastrointestinal conditions.

At low pH (<2), anthocyanins predominantly existed as the flavylium cation, a highly stable and strongly coloured form with a strong electron-donating ability. This structural form contributed significantly to radical scavenging capacity, particularly in DPPH and ABTS assays. During the stomach stage, this acidic environment preserved a large fraction of pigments. However, as pH increased to 7–8 in the intestinal phase, anthocyanins underwent structural rearrangements into quinoidal bases, chalcone pseudo-bases, and anhydro forms. These ring-opening transformations reduced their redox potential and altered their ability to donate electrons or hydrogen atoms, leading to diminished antioxidant responses. Encapsulation delayed pigment exposure to neutral pH, thereby limiting conversion into less active forms and preserving high antioxidant activity.[42]

DPPH and ABTS assays largely depend on radical scavenging, are more sensitive to structural changes and show high anthocyanin loss in non-encapsulated sohiong samples. However, FRAP assay values remained relatively high because the assay worked under acidic conditions, which favoured flavylium stability and reduced power. Overall, the observed results confirmed that microencapsulation stabilized anthocyanins by mitigating pH-driven structural changes and enzymatic degradation. The high antioxidant activity in encapsulated sohiong (SF-A300) reflected the preservation of flavylium cations and reduced conversion into chalcone forms, thereby maintaining strong radical scavenging and reducing capacity across digestion stages.[44]

3.4 Osmotic and photo oxidation activity

The results of assessing the osmotic stability for SA-F and SF-A300 revealed that, under intense osmotic stress for 180 min, SF-A300 showed a lower release of anthocyanins compared to SA-F. The wall matrix of SF-A300 calcium alginate, which prevented the premature release of anthocyanins in foods before ingestion, was demonstrated by the differences in anthocyanin release between SA-F and SF-A300. The osmotic force gradient was increased by variations in saline and sugar concentrations across entire membranes, leading to dehydration and interfering with hydrophobic interactions that maintain membrane stability. By forming a bridge with the carboxyl residues of alginate, calcium ions caused anthocyanins to leach.

To assess photo-oxidative stability, the SF-A and SF-A300 samples were tested under ultraviolet light (UV-C) at λ = 253.7 nm for 90 min for sterilisation, and it was determined whether SF-A was protected from photodegradation by the polymeric matrix. It was evident that UV-C radiation affected the total anthocyanin content in SF-A, as it increased with the time of exposure. Such an increase in the total anthocyanin content could result from the degradation of large anthocyanin molecules into small ones or from the release of anthocyanin compounds from glycosidic components. The total anthocyanin content from the SF-A300 samples was not significantly impacted by irradiation compared with that from SF-A. For SF-A exposed to UV-C light, TAC increased by 46.31% compared with the non-irradiated TAC from SF-A. This was due to the degradation of the fruit extract by UV light. However, when the TAC released from SF-A300 after irradiation was compared with that from SF-A, only a 3.95% increase in its value was observed at 90 min of exposure. After exposure to UV-C radiation for 90 min, the total anthocyanin content of empty microbeads treated with SA-P and SF-A300 decreased. The encapsulation, which shielded the entrapped polyphenols and provided a stronger stability profile than the non-encapsulated anthocyanins, was the reason for the improved stability of SF-A300.

4 Conclusion

In this study, laminar jet microencapsulation was successfully used to encapsulate anthocyanin extract from sohiong fruit, with alginate as a wall material. The process was optimized using RSM, and the SF-A300 nozzle produced microbeads with an average size of 588 ± 43 μm, with a consistent spherical shape and significant encapsulation efficacy (85.49%). Simulated *in vitro* digestion (SIVD) results demonstrated improved gastric stability, controlled-release profiles, improved bioaccessibility and enhanced physiological relevance. This study explained the mechanisms by which encapsulation synergistically preserved the bioactivity of anthocyanins and their functional efficacy under the influence of gastrointestinal and processing stressors. Future studies should focus on the limitations of this study, such as structural compatibility in real-life food systems, regulatory standardisation, shelf life, sensory evaluation and *in vivo* validation of metabolic activity, in order to facilitate the commercial translation of sohiong anthocyanins as stable, safe, and health-promoting bioactive compounds in functional food and nutraceutical applications.

Author contributions

Roshiya Nongmaithem: writing – original draft preparation; Raju Sasikumar: conceptualization, investigation, and data

curation; Kaviarasu G.: writing – original draft preparation; Selva Kumar T.: writing – review and editing; Ravikumar Rajarathinam: writing – original draft preparation; Paras Sharma: investigation and data curation; Sheena Haorongbam: writing – review and editing; Kowsalya T.; writing – original draft preparation; Senthilkumar K.: investigation and data curation; and Amit K. Jaiswal: conceptualization, writing – original draft preparation, review and editing and supervision.

Conflicts of interest

The authors have declared no conflicts of interest for this article.

Data availability

The data supporting this study are available from the corresponding author upon reasonable request.

References

1 H. Rymbai, R. Patel, N. Deshmukh, A. K. Jha and V. Verma, *Int. J. Minor Fruits Med. Aromat. Plants*, 2016, **2**, 54–56.
2 T. L. Swer, K. Chauhan, C. Mukhim, K. Bashir and A. Kumar, *LWT*, 2019, **114**, 108360, DOI: 10.1016/j.lwt.2019.108360.
3 S. Banerjee and A. Sen, *NBU J. Plant Sci.*, 2023, **15**, 31–38, DOI: 10.55734/nbujps.2023.v15i01.004.
4 T. L. Swer, K. Chauhan, P. K. Paul and C. Mukhim, *Int. J. Biol. Macromol.*, 2016, **92**, 867–871, DOI: 10.1016/j.ijbiomac.2016.07.105.
5 M. Yücetepe, Z. Tuğba Özaslan, M. Ş. Karakuş, M. Akalan, A. Karaaslan, M. Karaaslan and B. Başyiğit, *Food Res. Int.*, 2024, **187**, 114437, DOI: 10.1016/j.foodres.2024.114437.
6 L. Sunil and N. P. Shetty, *Appl. Microbiol. Biotechnol.*, 2022, **106**, 1783–1798, DOI: 10.1007/s00253-022-11835-z.
7 S. Chen, Y. Jia, Y. Wu and F. Ren, *Food Rev. Int.*, 2024, **40**, 3666–3689, DOI: 10.1080/87559129.2024.2369696.
8 I. Fernandes, A. Faria, C. Calhau, V. Freitas and N. Mateus, *J. Func. Foods*, 2014, **7**, 54–66, DOI: 10.1016/j.jff.2013.05.010.
9 A. Rezagholizade-shirvan, M. Soltani, S. Shokri, R. Radfar, M. Arab and E. Shamloo, *Food Chem.:X*, 2024, **24**, 101953, DOI: 10.1016/j.fochx.2024.101953.
10 V. Truong, P. T. Nguyen and V. T. Truong, *J. Food Process Eng.*, 2021, **44**, e13663, DOI: 10.1111/jfpe.13663.
11 M. Whelehan and I. W. Marison, *J. Microencapsul.*, 2011, **28**, 669–688, DOI: 10.3109/02652048.2011.586068.
12 K. Vivek, S. Mishra and R. C. Pradhan, *J. Food Process Eng.*, 2019, **42**, 12948, DOI: 10.1111/jfpe.12948.
13 R. Sasikumar, R. Nongmaithem, K. Vivek, S. Janghu, K. Govindasam and A. K. Jaiswal, *LWT*, 2024, **209**, 116796, DOI: 10.1016/j.lwt.2024.116796.
14 M. Giusti and R. E. Wrolstad, in *Handbook of Food Analytical Chemistry*, ed. L. Wrolstad, Wiley, Hoboken, 2005, ch. 18, pp. 19–31, DOI: 10.1002/0471709085.ch18.
15 T. Taghavi, H. Patel and R. Rafie, *Food Sci. Nutr.*, 2022, **10**, 2123–2131, DOI: 10.1002/fsn3.2065.
16 P. Pasukamonset, O. Kwon and S. Adisakwattana, *Food Hydrocol.*, 2016, **61**, 772–779, DOI: 10.1016/j.foodhyd.2016.06.039.
17 O. Aizpurua-Olaizola, P. Navarro, A. Vallejo, M. Olivares, N. Etxebarria and A. Usobiaga, *Food Chem.*, 2016, **190**, 614–621, DOI: 10.1016/j.foodchem.2015.05.117.
18 N. N. Gaikwad, A. Y. Kalal, S. K. Suryavanshi, P. G. Patil, D. Sharma and J. Sharma, *J. Food Process. Preserv.*, 2021, **45**, 15561, DOI: 10.1111/jfpp.15561.
19 C. M. Silva, A. J. Ribeiro, M. Figueiredo, D. Ferreira and F. Veiga, *AAPS J.*, 2005, **7**, 903–913, DOI: 10.1208/aapsj070488.
20 M. Minekus, M. Alminger, P. Alvito, S. Ballance, T. Bohn, C. Bourlieu, F. Carrière, R. Boutrou, M. Corredig, D. Dupont, C. Dufour, L. Egger, M. Golding, S. Karakaya, B. Kirkhus, S. L. Feunteun, U. Lesmes, A. Macierzanka, A. Mackie, S. Marze, D. J. McClements, O. Ménard, I. Recio, C. N. Santos, R. P. Singh, G. E. Vegarud, M. S. J. Wickham, W. Weitschies and A. Brodkorb, *Food Funct.*, 2014, **5**, 1113–1124, DOI: 10.1039/c3fo60702j.
21 L.-H. Pan, L.-P. Chen, C.-L. Wu, J.-F. Wang, S.-Z. Luo, J.-P. Luo and Z. Zheng, *Food Chem.*, 2022, **395**, 133626, DOI: 10.1016/j.foodchem.2022.133626.
22 R. Sasikumar, P. Sharma and A. K. Jaiswal, *Int. J. Food Eng.*, 2023, **19**, 1–13, DOI: 10.1515/ijfe-2022-0202.
23 R. Sasikumar, T. S. Kumar, K. Vivek, S. K. Panda and A. K. Jaiswal, *LWT*, 2025, **225**, 117929, DOI: 10.1016/j.lwt.2025.117929.
24 P. Mhlanga, S. M. Mianda and D. Sivakumar, *Foods*, 2024, **13**, 3562, DOI: 10.3390/foods13223562.
25 M. J. Mokale, S. Kesavan Pillai and D. Sivakumar, *Foods*, 2025, **14**, 2492, DOI: 10.3390/foods14142492.
26 A. De Prisco, D. Maresca, D. Ongeng and G. Mauriello, *LWT*, 2015, **61**, 452–462, DOI: 10.1016/j.lwt.2014.12.011.
27 I. Volf, M. Ignat, M. Neamtu and V. I. Popa, *Chem. Pap.*, 2014, **68**, 121–129, DOI: 10.2478/s11696-013-0417.
28 M. Kumar, A. Dahuja, A. Sachdev, C. Kaur, E. Varghese, S. Saha and K. V. S. S. Sairam, *Int. J. Biol. Macromol.*, 2019, **135**, 1070–1081, DOI: 10.1016/j.ijbiomac.2019.06.034.
29 S. Mohammadalinejhad, A. Almonaitytė, I. J. Jensen, M. Kurek and J. Lerfall, *Int. J. Biol. Macromol.*, 2023, **246**, 125684, DOI: 10.1016/j.ijbiomac.2023.125684.
30 L. Rayleigh, *Proc. Lond. Math. Soc.*, 1878, **10**, 4–13, DOI: 10.1112/plms/s1-10.1.4.
31 S. Mousavi and M. Siavashi, *Results Phys.*, 2025, **74**, 108305, DOI: 10.1016/j.rinp.2025.108305.
32 C. Bennacef, S. Desobry-Banon, L. Probst and S. Desobry, *Mar. Drugs*, 2023, **21**, DOI: 10.3390/md21040235.
33 M. L. Moya, M. Morley, O. Khanna, E. C. Opara and E. M. Brey, *J. Mater. Sci. Mater. Med.*, 2012, **23**, DOI: 10.1007/s10856-012-4575-9.
34 A. P. Santos, S. S. Chevallier, B. de Haan, P. de Vos and D. Poncelet, *J. Biomater. Appl.*, 2021, **36**, 638–647, DOI: 10.1177/0885328221988979.
35 N. Almassri, F. J. Trujillo, A. V. Klieve, R. Bell, D. Ying and N. Shiferaw Terefe, *Bioengineering*, 2025, **12**, 1341, DOI: 10.3390/bioengineering12121341.

36 I. Ćorković, A. Pichler, I. Ivić, J. Šimunović and M. Kopjar, *Gels*, 2021, **7**, 231, DOI: 10.3390/gels7040231.
37 M. Jiang and Y. Zhang, *J. Agric. Food Res.*, 2023, **11**, 100488, DOI: 10.1016/j.jafr.2022.100488.
38 A. Mahajan, P. Sharma, G. Goudar, P. Gogoi, R. Sasikumar, S. Kalpuri and T. Longvah, *Discov. Food*, 2025, **6**, 12, DOI: 10.1007/s44187-025-00714-x.
39 H. Ayvaz, T. Cabaroglu, A. Akyildiz, C. U. Pala, R. Temizkan, E. Ağçam, Z. Ayvaz, A. Durazzo, M. Lucarini, R. Direito and Z. Diaconeasa, *Antioxidants*, 2022, **12**, 48, DOI: 10.3390/antiox12010048.
40 C. Fredes, M. J. Osorio, J. Parada and P. Robert, *LWT*, 2018, **91**, 549–556, DOI: 10.1016/j.lwt.2018.01.090.
41 Y. Chen, H. Chen, W. Zhang, Y. Ding, T. Zhao, M. Zhang, G. Mao, W. Feng, X. Wu and L. Yang, *Food Funct.*, 2019, **10**, 6052–6061, DOI: 10.1039/c9fo00871c.
42 J. Correa-Betanzo, E. Allen-Vercoe, J. McDonald, K. Schroeter, M. Corredig and G. Paliyath, *Food Chem.*, 2014, **165**, 522–531, DOI: 10.1016/j.foodchem.2014.05.135.
43 Y. Jang and E. Koh, *Food Chem.*, 2024, **434**, 137443, DOI: 10.1016/j.foodchem.2023.137443.
44 L. Liang, X. Wu, T. Zhao, J. Zhao, F. Li, Y. Zou, G. Mao and L. Yang, *Food Res. Int.*, 2012, **46**, 76–82, DOI: 10.1016/j.foodres.2011.11.024.